

See discussions, stats, and author profiles for this publication at: <https://www.researchgate.net/publication/231705019>

pH Dependence of Macroscopic Swelling and Microscopic Structures for Thermo/pH-Sensitive Gels with Different Charge Distributions

ARTICLE *in* MACROMOLECULES · NOVEMBER 2008

Impact Factor: 5.8 · DOI: 10.1021/ma801042q

CITATIONS

9

READS

22

4 AUTHORS, INCLUDING:



[Mitsuhiro Shibayama](#)

The University of Tokyo

322 PUBLICATIONS 8,771 CITATIONS

SEE PROFILE

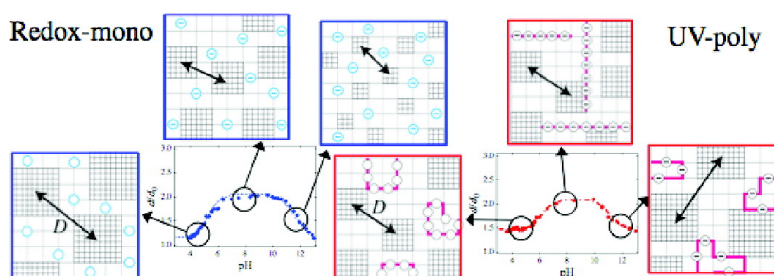
Article

pH Dependence of Macroscopic Swelling and Microscopic Structures for Thermo/pH-Sensitive Gels with Different Charge Distributions

Takuya Suzuki, Takeshi Karino, Fumiyoshi Ikkai, and Mitsuhiro Shibayama

Macromolecules, **2008**, 41 (24), 9882-9889 • Publication Date (Web): 17 November 2008

Downloaded from <http://pubs.acs.org> on December 23, 2008



More About This Article

Additional resources and features associated with this article are available within the HTML version:

- Supporting Information
- Access to high resolution figures
- Links to articles and content related to this article
- Copyright permission to reproduce figures and/or text from this article

[View the Full Text HTML](#)



ACS Publications
High quality. High impact.

Macromolecules is published by the American Chemical Society, 1155 Sixteenth Street N.W., Washington, DC 20036

pH Dependence of Macroscopic Swelling and Microscopic Structures for Thermo/pH-Sensitive Gels with Different Charge Distributions

Takuya Suzuki,[†] Takeshi Karino,[†] Fumiyoshi Ikkai,[‡] and Mitsuhiro Shibayama^{*,†}

Institute for Solid State Physics, The University of Tokyo, 5-1-5 Kashiwanoha, Kashiwa, Chiba 277-8581, Japan, and Nihon L'Oreal K.K., KSP R&D-D637, 3-2-1 Sakado, Takatsu-ku, Kawasaki, Kanagawa 213-0012, Japan

Received May 8, 2008; Revised Manuscript Received September 26, 2008

ABSTRACT: The pH dependence of the microstructure formation of three types of polymer gels that consist of *N*-isopropylacrylamide (NIPAm) and acrylic acid (AAc) but have different architectures was investigated by means of macroscopic swelling measurements and microscopic small-angle neutron scattering. The first type was an NIPAm/AAc copolymer gel in which NIPAm and AAc monomers were randomly copolymerized by redox polymerization (redox-mono). The second type was an ultraviolet (UV)-cross-linked NIPAm/poly-AAc copolymer gel in which NIPAm monomer was copolymerized with poly(acrylic acid) (UV-poly). The third type was a mixture of poly-NIPAm gel and poly-AAc in which the poly-NIPAm network was prepared by redox polymerization in the presence of cross-linker, whereas poly-AAc was physically entrapped in the poly-NIPAm polymer network (redox-poly). These three types of gels contain the same amount of AAc but different spatial configurations. The following conclusions were obtained: (1) Redox-mono and UV-poly showed swelling behavior in the middle pH range (i.e., pH 6–10) because of the ionization of AAc. Redox-poly did not show such a swelling behavior over all pHs. (2) SANS analyses confirmed that redox-mono and UV-poly, which exhibit similar swelling behaviors, had marked pH dependence in the gel microstructure because of different architectures and spatial distributions of charged AAc groups.

Introduction

Ionic hydrogel is one of the most functional gels not only because it can absorb a large amount of water but also because a small change in the degree of ionization can dramatically affect its swelling degree and transparency.^{1–7} In general, an introduction of ionic groups to a neutral polymer gel leads to improvement in transparency and swelling. This phenomenon has been explained as being a result of the effects of electrostatic repulsion and the osmotic pressure of counterions.^{4,8–11} These effects play essential roles in determining not only the macroscopic equilibrium swelling degree but also the microscopic network structures. In regards to the microscopic structures of gels, inhomogeneities in gels have been extensively investigated during the past two decades theoretically¹² and by the use of scattering methods.¹³ In particular, those in charged gels have been intriguing problems as reported with various scattering methods such as static light scattering (SLS),^{14,15} dynamic light scattering (DLS),^{16,17} small-angle X-ray scattering (SAXS),^{14,18} and small-angle neutron scattering (SANS).^{3,19,20} However, none of these works have focused on the spatial distribution of the charged groups in the network.

In this series of articles, we explored the microstructure and dynamics of thermo/pH-sensitive polymer gels consisting of thermosensitive *N*-isopropylacrylamide and pH-sensitive acrylic acid comonomer (NIPAm/AAc) with different architectures,^{21,22} where AAc comonomers were distributed either (1) randomly as a monomer unit (redox-mono), (2) sequentially as a poly-AAc chains (UV-poly), or (3) physically entrapped in a poly-NIPAm network (redox-poly). It is known that NIPAm gels undergo a continuous volume phase transition at ~33 °C because of hydrophobic interactions.²³ The volume phase transition of NIPAm/AAc gels becomes discontinuous by the introduction of charged AAc comonomer, and the transition

temperature shifts upward.¹ Microscopically, it corresponds to microphase separation with a repeat distance of a few hundred angstroms. The origin of microphase separation was successfully explained as being a balance of enthalpic and entropic driving forces, that is, macroscopic shrinking by hydrophobic interaction versus swelling due to the requirement of the uniform spatial distribution of counterions. As a result, the system chooses a microphase separation. In the first article of this series,²¹ we discussed the temperature dependence of the microstructure for the above-mentioned three types of gels with different distributions of charged groups, following the difference of effective cross-linking density between redox- and UV-induced polymerized gels by swelling measurements. In the second article, these microstructure formations were studied by DLS and swelling measurements from the viewpoints of both static inhomogeneities and dynamic fluctuations.²² On the basis of these studies, it was concluded that quite different gel microstructures were formed by depending on different spatial configurations of ionizable groups in polymer gels. Redox-mono has a higher effective degree of ionization than does UV-poly because counterion condensation along poly-AAc chains occurs in the latter. The counterion condensation also results in lowering the gel volume transition temperature of UV-poly in contrast with that of redox-mono. However, one of the most important aspects of charged gels, that is, pH dependence, has not been investigated so far.

To clarify the roles of ionized groups in these gels, we studied here the pH dependence of microscopic network structures. Emphasis was on the discussion about the pH dependence of (1) the macroscopic ionization effect below the volume phase transition temperature by observation of swelling behavior and of (2) microscopic inhomogeneities of polymer networks above and below the volume phase transition temperature.

Theoretical Background

Elastic Behavior. The elastic modulus, E , can be determined from the slope of linear dependence at a low strain region by the equation

* To whom correspondence should be addressed. E-mail: shibayama@issp.u-tokyo.ac.jp.

[†] The University of Tokyo.

[‡] Nihon L'Oreal K.K.

$$\sigma = E(\lambda - \lambda^{-2}) \quad (1)$$

where σ is the applied stress and λ is the relative deformation ratio (deformed length/initial length). For an affine network model, the effective cross-linking density, ν_e , is determined using the equation^{8,24}

$$E = RT\phi_0^{2/3}\phi^{1/3}\nu_e \quad (2)$$

where R , T , ϕ_0 , and ϕ are the gas constant, the absolute temperature, and the polymer volume fraction in the sample preparation and in the swollen state, respectively. Because ϕ equals ϕ_0 just after the sample preparation, eq 2 becomes

$$E = RT\phi_0\nu_e \quad (3)$$

From the elastic measurement just after the sample preparation, we can obtain ν_e by using the value of E with eqs 1 and 3.

Swelling Behavior. The osmotic pressure, Π , of a charged gel is given by^{8,25}

$$\Pi = \Pi_{\text{mix}} + \Pi_{\text{el}} + \Pi_{\text{ion}} \approx -\frac{\Delta\mu}{V_s} \quad (4)$$

where V_s is the molar volume of the solvent and $\Delta\mu$ is the chemical potential change by gel swelling. Π_{mix} , Π_{el} , and Π_{ion} are the contributions to the osmotic pressure due to polymer–solvent mixing, polymer chain elasticity, and Donnan potential, respectively. In the context of conventional theories for swelling,⁸ Π_{mix} is given as a function of the polymer volume fraction, ϕ , by

$$\Pi_{\text{mix}} = -\frac{RT}{V_s}[\phi + \ln(1 - \phi) + \chi\phi^2] \quad (5)$$

where χ is the Flory–Huggins interaction parameter.

Π_{el} is given by

$$\Pi_{\text{el}} = \nu_e RT \left[\frac{1}{2} \left(\frac{\phi}{\phi_0} \right) - \left(\frac{\phi}{\phi_0} \right)^{1/3} \right] \quad (6)$$

The theoretical value of cross-linking density, ν_t , is stoichiometrically given by²⁶

$$\nu_t = \frac{fC_{\text{cl}}}{2C_0} \frac{\phi}{V_{\text{NIPA}}} = \frac{fC_{\text{cl}}}{2} \quad (7)$$

where f , C_{cl} , C_0 , and V_{NIPA} are the functionality of cross-linking, the feed concentration of the cross-linkers, the initial monomer concentration, and the molar volume (dm^3/mol) of the NIPAm monomeric unit, respectively.

The osmotic pressure generated by Donnan potential is given by¹¹

$$-\frac{\Delta\mu_{\text{ion}}}{V_s} \approx RT\Delta C \quad (8)$$

where ΔC is the difference in the mobile ion concentrations between the inside and outside of the gel,^{4,27,28} that is

$$\Delta C \approx ([\text{Na}^+]_{\text{in}} + [\text{OH}^-]_{\text{in}}) - ([\text{Na}^+]_{\text{out}} + [\text{OH}^-]_{\text{out}}) \quad (\text{for } \text{pH} > 7)$$

$$\Delta C \approx ([\text{H}^+]_{\text{in}} + [\text{Cl}^-]_{\text{in}}) - ([\text{H}^+]_{\text{out}} + [\text{Cl}^-]_{\text{out}}) \quad (\text{for } \text{pH} < 7) \quad (9)$$

Because of the osmotic balance of mobile ion and electro-neutrality, ΔC is given by⁴

$$\Pi_{\text{ion}} = \Delta C \approx \sqrt{[\text{COO}^-]^2 + 4I^2} - 2I \quad (10)$$

where $[\text{COO}^-]$ is the concentration of the ionized AAc groups and I is the ionic strength of the system. Here $[\text{COO}^-]$ is given by

$$[\text{COO}^-] = \alpha f_{\text{AAc}} C_0 \left(\frac{\phi}{\phi_0} \right) \quad (11)$$

where α is the degree of ionization of AAc groups and f_{AAc} is the fraction of AAc groups in the polymer networks. α is related to pH by the Henderson–Hasselbalch equation^{29,30}

$$\text{pH} = \text{p}K_a - n_0 \log \frac{1 - \alpha}{\alpha} \quad (12)$$

where K_a is the dissociation constant of AAc. From eq 12, the following equation is obtained

$$\alpha = \frac{1}{10^{(\text{p}K_a - \text{pH})/n_0} + 1} \quad (13)$$

It is convenient to employ the linear swelling degree, d/d_0 , where d and d_0 are the gel diameter at the observation and that at the gel preparation, respectively. The swelling degree and the volume swelling ratio can simply be related by

$$\frac{d}{d_0} = \left(\frac{\phi_0}{\phi} \right)^{1/3} \quad (14)$$

By imposing a condition of $\Pi = 0$ and using eqs 4–6, 10, and 14, we can theoretically obtain d/d_0 as a function of pH.

Rabin–Panyukov Theory for Small-Angle Neutron Scattering. The microphase separation of weakly charged gels is described by the Rabin–Panyukov theory (RP theory).^{12,31,32}

The RP theory properly describes the frozen inhomogeneities on the basis of a mean-field theory of polymer gels. The theoretical structural factor, $S(q)$, consists of two contributions, one from the static inhomogeneities, $C(q)$, and the other from the thermal concentration fluctuations, $G(q)$, where q is the scattering vector. Both $C(q)$ and $G(q)$ are built up with well-defined parameters, that is, the average degree of polymerization between cross-links (N), the polymer volume fraction (ϕ), the degree of ionized charged groups ($f = \alpha f_{\text{AAc}}$), and T (or the Flory's interaction parameter, χ). Here we define N as $N = [(C_0 + 2C_{\text{cl}})/2C_{\text{cl}}]$. Using two sets of parameters, that is, those at sample preparation (ϕ_0, f_0, χ_0), in addition to those at observation (ϕ, f, χ), $S(q)$ is given by eqs 15–17

$$S(q) = G(q) + C(q) \quad (15)$$

$$G(q) = \frac{\phi N g(q)}{1 + w(q)g(q)} \quad (16)$$

$$C(q) = \frac{\phi N}{[1 + w(q)g(q)]^2(1 + Q^2)^2} \times \left[6 + \frac{9}{w_0(q) - 1 + (1/2)Q^2(\phi_0/\phi)^{2/3}\phi_0^{-1/4}} \right] \quad (17)$$

where the subscript 0 means the parameter value at sample preparation, $Q (= aN^{1/2}q)$ is the dimensionless wave vector, and a and $w(q)$ denote the segment length (8.12 Å for NIPAm polymer chains)^{19,33} and the effective second virial coefficient, respectively. The function of $g(q)$ is given by eq 18

$$g(q) = \frac{1}{Q^2/2 + (4Q^2)^{-1} + 1} + \frac{2(\phi/\phi_0)^{2/3}\phi_0^{1/4}}{(1 + Q^2)^2} \quad (18)$$

The functions of $w(q)$ and $w_0(q)$ are expressed by eqs 19 and 20, respectively

$$w(q) = (1 - 2\chi + \phi)\phi N + \frac{l_B f^2 \phi N^2}{Q^2 + l_B f \phi N} \quad (19)$$

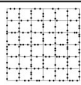
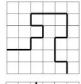
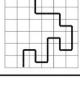
$$w_0(q) = \phi_0^{5/4} N + \frac{l_B f_0^2 \phi_0^{5/4} N^2}{Q^2(\phi_0/\phi)^{2/3} + l_B f_0 \phi_0^{5/4} N} \quad (20)$$

l_B is the dimensionless Bjerrum length given by $l_B = 4\pi L_B/a$, where L_B is the Bjerrum length set at 7 Å for aqueous solutions at 25 °C.¹⁹

Experimental Section

Samples. *N*-isopropylacrylamide (NIPAm), acrylic acid (AAc), *N,N'*-methylene bisacrylamide (BIS), ammonium persulfate (APS),

Table 1. Sample Code, Concentrations, and Diagram Models

Code	C_{NIPAm} (mM)	C_{AAc} (mM)	C_{BIS} (mM)	C_{APS} (mM)	C_{TEMED} (μL)	Schematic Diagrams
Redox-mono	668	32	7	1.54	24	
UV-poly	668	32*	0	20	0	
Redox-poly	668	32*	7	1.54	24	

* C_{AAc} was calculated in monomer units.

and N,N,N',N' -tetramethyl ethylenediamine (TEMED) were purchased from Wako Chemical, Tokyo. NIPAm and AAc were purified before use by recrystallization and distillation, respectively. Poly-AAc ($M_w = 118\,000$) was purchased from Polymer Source, Canada, and was used without further purification.

Gel Preparation. Three types of NIPAm/AAc copolymer gel were prepared using two polymerization methods. Details of the concentrations of each component and the schematic diagrams of network architectures are given in Table 1. In the schematic diagrams, the thin gray lattice-shaped boxes, the black dots, and the black lines represent poly-NIPAm chains, AAc monomers, and poly-AAc chains, respectively. The first type is a NIPAm/AAc copolymer gel in which NIPAm and AAc monomers are randomly copolymerized by the use of conventional redox polymerization (code: redox-mono). The second type is a NIPAm/poly-AAc copolymer gel in which poly-AAc is copolymerized with NIPAm by UV-induced polymerization method (code: UV-poly). The third type is a NIPAm/poly-AAc polymer gel prepared from NIPAm and poly-AAc by the use of a redox polymerization method in which poly-AAc chains are physically entrapped in the NIPAm network without copolymerization with NIPAm (code: redox-poly). Note that these three types of gels have the same monomer concentrations of AAc (32 mM) and NIPAm (668 mM) but different spatial configurations of AAc groups. In addition to these gel samples, NIPAm homopolymer gels were prepared using either redox or UV-induced polymerization for the estimation of ν_e and the reference values of χ and C_{el} for noncharged gels (code: redox-NIPAm, UV-NIPAm, respectively). The preparation process for each type of gel was as follows.

(Redox-mono): Prescribed amounts of NIPAm and AAc were dissolved in 10 mL of deionized water in a test tube. Then, BIS and APS were added to the solution as a cross-linker and redox initiator, respectively. The concentrations of NIPAm, AAc, BIS, and APS were 668, 32, 7, and 1.54 mM, respectively. After the further addition of 24 μL of TEMED as an accelerator, the solution was kept at 20 °C for 24 h for gel maturing.

(UV-poly): An aqueous solution containing NIPAm, AAc polymer ($M_w = 118\,000$ and $M_w/M_n = 1.13$, M_w and M_n being the weight- and number-average molecular weights, respectively), and APS (as UV photoinitiator) was exposed to UV radiation provided by a 500 W deep UV lamp (USHIO, Tokyo, Japan) with an illuminance spectrum including a range of wavelengths of <300 nm. The concentrations of NIPAm, AAc polymer, and APS were 668, 32 (expressed as monomer units), and 20 mM, respectively. UV irradiation was carried out by the use of a parallel light irradiated from the side of the test tube. The optical density of the pregel solution was ~ 0.7 at 254 nm. Transparent gels were thus obtained by UV irradiation for 1 h at 20 °C. We note that the UV-induced polymerization of NIPAm monomers and poly-AAc without any cross-linkers such as BIS as well as degradation had been reported by Ikkai et al.^{35,36}

(Redox-poly): Prescribed amounts of NIPAm, AAc polymer, BIS, and APS, were dissolved in 10 mL of deionized water in a test tube. The concentrations of NIPAm, AAc polymer, BIS, and

APS were 668, 32 (expressed as monomer units), 7, and 1.54 mM, respectively. After the further addition of 24 μL of TEMED as an accelerator, the solution was kept at 20 °C for 24 h for gel maturing.

(Redox-NIPAm): NIPAm was dissolved in 10 mL of deionized water in a test tube. Then, BIS and APS were added to the solution as the cross-linker and redox initiator, respectively. The concentrations of NIPAm, BIS, and APS were 700, 7, and 1.54 mM, respectively. After the further addition of 24 μL of TEMED as an accelerator, the solution was kept at 20 °C for 24 h for gel maturing.

(UV-NIPAm): An aqueous solution containing 700 mM NIPAm and 20 mM APS (as UV photoinitiator) was exposed to UV-irradiation for 1 h at 20 °C.

The polymerizations of all gel samples were carried out at pH 8 where AAc was ionized.

Compression Measurements. Before pH dependence experiments, the difference in the elastic modulus and the effective cross-linking densities between redox and UV-induced polymerized gels was measured for redox-NIPAm and UV-NIPAm. Uniaxial compression measurements were carried out using a universal testing machine (EZ-test, Shimadzu, Kyoto, Japan). The cylindrical samples were prepared as discussed above. The diameter and height of redox-NIPAm were 27 and 6.4 mm, and those of UV-NIPAm were 10 and 4.5 mm, respectively. Each compression measurement was carried out just after the sample preparation in a thermostatted room at 20 °C in <1 min to avoid the evaporation of water in the gels. The crosshead speed was 10 mm/min.

Swelling Degree Measurements. For swelling measurements, all gel samples were prepared in a narrow quartz capillary (800 μm diameter). The prepared gels with cylindrical shape were taken from the quartz capillaries and washed with an excess amount of water. The sample was immersed in a thermostatted chamber filled with distilled water. The swelling degree, d/d_0 , was measured by monitoring the diameter of the cylindrical gel, d , via an inverted microscope (TMD300, Nikon, Tokyo, Japan) coupled to an image processor (Algas 2000, Hamamatsu Photonics, Hamamatsu, Japan). The pH of the solution was carefully controlled by the outlet of the flow adjusted by HCl(aq) for pH < 7 and NaOH(aq) for pH > 7 at $T = 25$ °C. When the shape of a gel became irregular upon swelling or shrinking, the maximum width of the gel was measured. The measurement was repeated at least three times, and its average was employed as the value d .

Small-Angle Neutron Scattering. SANS experiments were carried out using the 2D SANS spectrometer (SANS-U) of the Institute for Solid State Physics of the University of Tokyo.³⁷ The SANS intensity functions were collected in a wide temperature range for 1.5 and 8 h at a 2 and 8 m sample-to-detector distance, respectively. Gel samples in quartz cells with a 4 mm optical path were irradiated with a 7.0 Å wavelength neutron beam. Incoherent scattering subtraction was carried out with the method reported by Shibayama et al.³⁸ For SANS measurements, all prepared gels were taken out of the test tubes and smashed through a 500 μm sieve. Then, gels were washed with a large amount of water for 3 days under stirring, and freeze drying was carried out. The gel volume fraction was fixed to be $\phi = 0.1$ to suppress the change in inhomogeneities resulting from the change in polymer concentration with increasing temperature. For pD-adjusted gels, a D₂O solution with the predetermined pD adjusted by DCl(aq) or NaOD(aq) was added to the freeze-dried gel to be a pH* of 4, 6, 8, or 11, where pH* is the direct reading in a D₂O solution by a conventional pH meter. We should consider the fact that the pH in an H₂O solution is different from its corresponding pD in a D₂O solution. The relationship between pD and pH* is generally expressed as $\text{pD} = \text{pH}^* + 0.41$.³⁹ This relation was employed in the discussion of SANS results. SANS profiles were obtained at 25, 33, 37, 41, and 45 °C.

Results and Discussion

Compression Measurements. Prior to the discussion about the pH dependence of the three types of NIPAm/AAc copolymer gels, let us show the difference in the elastic behavior between

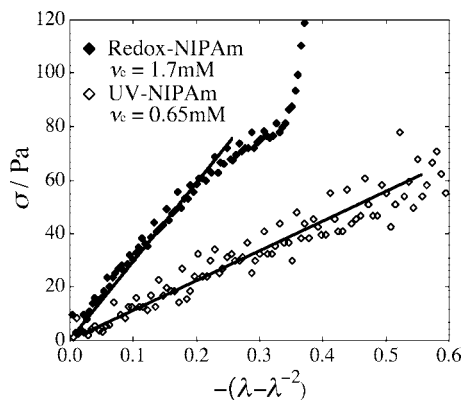


Figure 1. Stress–strain curves for redox-NIPAm and UV-NIPAm under a sample preparation condition.

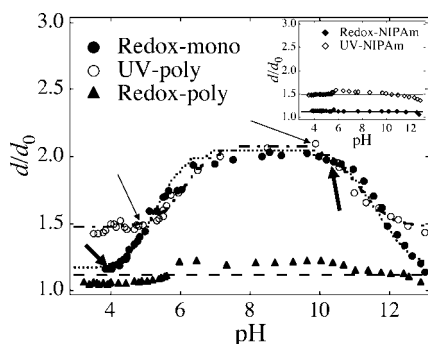


Figure 2. pH dependence of the linear swelling ratio, d/d_0 , and the corresponding fits for redox-mono (●, ---), UV-poly (○, ---), and redox-poly (▲, ---). The inset shows d/d_0 for redox-NIPAm (◆) and UV-NIPAm (◇).

redox and UV-induced polymerized gels. Figure 1 shows the stress–strain data for redox-NIPAm and UV-NIPAm. σ of each sample showed a linear dependence of strain in the low-strain regions, as shown by the solid line obtained with eqs 1 and 3. It can be easily seen from the slope that redox-NIPAm is more rigid than UV-NIPAm. This means that more cross-links are formed in redox polymerized gels than in UV-induced polymerized gels, which was also shown in our previous article of the temperature dependence of swelling degree measurement.²¹ We calculated ν_e from the slope and eq 3. The obtained ν_e values were 1.7 and 0.65 mM for redox-NIPAm and UV-NIPAm, respectively. We later discuss the ν_e in detail by the comparison with the theoretical values.

Swelling Degree Measurements. Figure 2 shows the pH dependence of the swelling degree of redox-mono, UV-poly, and redox-poly at 25 °C. Different pH dependences in d/d_0 were observed among the three types of gels. d/d_0 started to increase at ca. pH 4 for redox-mono (thick arrow) and ca. pH 5 for UV-poly (thin arrow) and reached a plateau at pH 7 and then started to decrease at a pH of about 10 (thick and thin arrows, respectively, for redox-mono and UV-poly). Because the pK_a of AAc monomer is well known to be 4.25,⁴⁰ the increase in d/d_0 above pH 4 is due to the ionization of AAc and the increase in the osmotic pressure. The decrease above pH 10 is due to electrostatic screening effect by the added NaOH. (See eq 10.) Although d/d_0 for redox-poly seemed to increase slightly in the range of pH 6 and 11, the pH effect is much smaller than others. This means that physical entrapment of poly-AAc does not produce significant Donnan potential even if poly-AAc is fully ionized. The inset shows the swelling behaviors for noncharged redox-NIPAm and UV-NIPAm, which have no pH dependence. Note that the swelling degrees are different between the two (i.e., $d/d_0 \approx 1.1$ for redox-NIPAm and 1.5 for UV-NIPAm).

This means that the former has a higher cross-linking density than the latter, as shown in the Figure 1.

Another interesting fact is that the pH values where d/d_0 started to increase or decrease are different between redox-mono and UV-poly. In particular, the starting point of swelling for UV-poly shifted to a higher pH than that for redox-mono. That is, at pH < 7, AAc groups of redox-mono become ionized more easily with increasing pH than those of UV-poly because of the uniform distribution of AAc in monomer units. At pH > 7 the d/d_0 of UV-poly decreased more easily with increasing pH than that of redox-mono because of the localization of AAcs and surrounding Na^+ resulted in the stronger screening effect (i.e., the so-called counterion condensation).^{41,42}

We theoretically calculated the swelling degrees by using eqs 4–7, 10, and 14 by solving $\Pi = 0$ under the condition of $\nu_e = \nu_t$. Here, the following parameters were fixed: $V_s = 0.018 \text{ dm}^3/\text{mol}$, $f = 4$, $C_0 = 700 \text{ mM}$, $n_0 = 1$, and $f_{AAc} = 0.0457 (= 32/700)$ for redox-mono and 0.0184 for UV-poly (chain line), respectively.^{4,21} The calculation was carried out as follows: First, χ and C_{cl} of redox-polymerized gels (redox-mono and redox-poly) and UV-induced gels (UV-poly) were estimated on the basis of the d/d_0 of redox-NIPAm and UV-NIPAm, respectively, with eqs. 4–7 and 14. Note that d/d_0 does not have any pH dependence in the calculation without the use of eq 10. By substituting the thus obtained χ and C_{cl} , we calculated d/d_0 and estimated pK_a values. The evaluated χ and C_{cl} were $\chi = 0.47$ and $C_{cl} = 5.0 \text{ mM}$ for redox-mono and $\chi = 0.43$ and $C_{cl} = 2.0 \text{ mM}$ for UV-poly. These calculated values agreed well with the experimental results, as denoted by the lines in the figure. The fact that $\chi < 0.5$ means that these gels are in a good solvent at 25 °C. The C_{cl} of UV-poly is lower than that of redox-mono, as discussed so far.

Now let us mention the validity of the obtained C_{cl} values. It is obvious that C_{cl} of redox-polymerized gel is close to the feed concentration (i.e., 7 mM). However, the ν_t value given by eq 7 is much greater than the ν_e value discussed in Figure 1. There have been many studies of the comparison between ν_t and ν_e by not only swelling measurements but also compression measurements. As far as we know, in the case of the compression measurements, many researchers have shown that ν_e is about one or two orders of magnitude less than ν_t .^{43–46} For instance, Gundogan et al. showed the difference between ν_t and ν_e and indicated that the 70–85% of BIS can be wasted during the polymerization.⁴³ Xue et al. also showed the much lower value of ν_e than that of ν_t in NIPAm/AAc gels.⁴⁴ In the case of swelling behavior, the entanglement of polymer chains by swelling is considered to play an important role, resulting in additional cross-linking points.^{26,47} Shibayama et al. showed this effect for NIPAm gel and theoretically explained the swelling behavior by employing ν_t .²⁶ The entanglement effect was also studied with Monte Carlo simulations.⁴⁸ Moreover, Tokuyama et al. recently clarified that ν_e values of swollen NIPAm gels are even higher than ν_t values because of the chain entanglement.⁴⁹ Therefore, the difference between ν_e by compression measurements and ν_t by swelling measurements in our experimental results stands to reason, and these results strongly support the additional cross-linking effects. In addition, it is noteworthy that the ratio of redox-NIPAm to UV-NIPAm about ν_e is almost the same as that about ν_t (~ 2.5).

As for the curve fitting results of pK_a values, the obtained pK_a values were 5.3 and 6.1 for redox-mono and UV-poly, respectively. These pK_a values are obviously larger than the pK_a of AAc (= 4.25). It is conjectured that the ionization tendency is suppressed depending on the degree of containment of AAc groups in the NIPAm networks in the order of redox-mono < UV-poly. The suppression of the ionization tendency of AAc groups in UV-poly is probably due to the localization

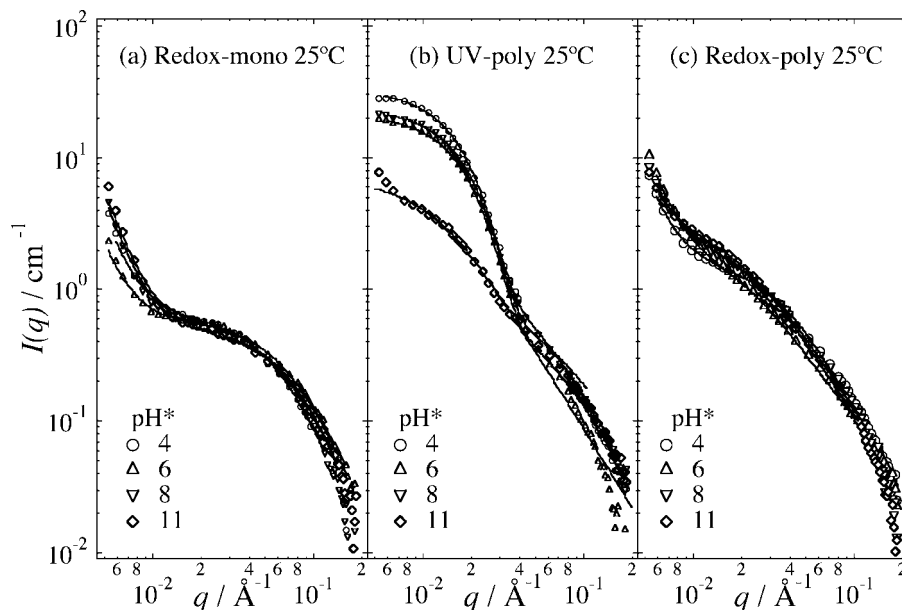


Figure 3. pH* dependence of SANS profiles for (a) redox-mono, (b) UV-poly, and (c) redox-poly at $T = 25\text{ }^{\circ}\text{C}$. The solid lines denote the results of curve fitting.

of ionizable groups along the poly-AAc chains as well as hydrogen bonding between poly-AAc chains. The swelling behavior of redox-poly could not be reproduced by the above equations and was rather reproduced by that for redox-NIPAm (i.e., noncharged NIPAm gels).

Small-Angle Neutron Scattering Results. Figure 3 shows the pH* dependence of SANS profiles, $I(q)$, at $T = 25\text{ }^{\circ}\text{C}$ for redox-mono, UV-poly, and redox-poly. Here the solid lines in the Figure denote theoretical fitting curves described below. We note that $I(q)$ values of UV-poly at pH* of 4, 6, and 8 are much higher than those of redox-mono and redox-poly, indicating that larger static inhomogeneities exist in UV-poly than in the others. In addition, the shapes of $I(q)$ values are very different from others, and $I(q)$ values have a broad shoulder around $q \approx 0.01\text{ }\text{\AA}^{-1}$. This is ascribed to the localization of ionizable groups in the gel network as polymer chains, that is, poly-AAc, and the counterion condensation occurs near poly-AAc, as discussed in the previous article.²¹ We discuss here the pD (or pH*) dependence of SANS profiles for each type of gels because the temperature dependence has already been discussed in our previous article.²¹ At a low temperature range (i.e., $T = 25\text{ }^{\circ}\text{C}$), no remarkable pH* dependence was observed except for pH* of 11 in UV-poly. The very low pH* dependence in the SANS profiles is due to the following facts. SANS measurements were carried out under a fixed volume condition ($\phi = 0.1$). As a result, swelling-causing force due to the ionized AAc groups was suppressed, and the SANS curves became insensitive to pH*. Note that the SANS curve for UV-poly at pH* of 11 is similar to those of redox-poly at any pH*, suggesting that a strong electrostatic screening effect occurred at pH* of 11 in UV-poly because of the lower degree of ionization than that in redox-mono.

Now let us discuss the results of curve fitting at $T = 25\text{ }^{\circ}\text{C}$. In the case of redox-mono, an obvious upturn was observed at low- q regions, indicating the frozen-in structural inhomogeneities discussed by Horkay et al. At $T = 25\text{ }^{\circ}\text{C}$ (i.e., in the lower temperature region before the volume phase transition occurs), $I(q)$ was well fit with a modified squared-Lorentz (SL) function^{50–52}

$$I(q) = \frac{I_L(0)}{1 + \xi^2 q^2} + \frac{I_{SL}(0)}{(1 + \xi^2 q^2)^2} + I_e(0)q^{-3.6} \quad (21)$$

Here the second term of the right-hand side of eq 21 is based on the so-called Debye–Bueche function, and ξ denotes a correlation length of concentration fluctuations in the gel network. $I_L(0)$ and $I_{SL}(0)$ are the zero- q intensities corresponding to the dynamic and static contributions to $I(q)$. The fitted ξ value was $\sim 10\text{ }\text{\AA}$. We note that the ξ value increased until $20\text{ }\text{\AA}$ at $41\text{ }^{\circ}\text{C}$ with increasing temperature, meaning the increase in concentration fluctuation of polymer networks.

In the case of UV-poly, $I(q)$ showed a convex curve at $q \leq 0.03\text{ }\text{\AA}^{-1}$, indicating the macroscopic structural inhomogeneities. Such functions are no longer fit with the SL plot but rather the phenomenological Gauss–Lorentz (GL) plot, which is given by^{14,53,54}

$$I(q) = \frac{I_L(0)}{1 + \xi^2 q^2} + I_G(0) \exp\left(-\frac{R_g^2 q^2}{3}\right) \quad (22)$$

where the existence of randomly distributed static inhomogeneities of polymer networks with a characteristic mean size of R_g is assumed, as shown by the second term of the right-hand side of eq 22. As the fitting results, structural parameters such as ξ and R_g showed no significant pH* dependence. At any pH*, the fitted ξ and R_g were about 20 and $100\text{ }\text{\AA}$ at $T = 25\text{ }^{\circ}\text{C}$ and then increased to 160 and $120\text{ }\text{\AA}$ at $T = 33\text{ }^{\circ}\text{C}$ because of the increase in microscopic inhomogeneities.

In the case of redox-poly, SANS profiles were almost the same as homopolymer gels irrespective of pH*. Indeed, $I(q)$ values were well fit to eq 21 without showing remarkable pH* dependence of the fitted ξ ($= 30\text{ }\text{\AA}$ at $25\text{ }^{\circ}\text{C}$ and $60\text{ }\text{\AA}$ at $33\text{ }^{\circ}\text{C}$, irrespective of pH*). Therefore, we can conclude that the physically trapped poly-AAc chains did not affect microscopic inhomogeneities.

Figure 4 shows the pH* dependence of SANS profiles, $I(q)$, for redox-mono at $T = 45\text{ }^{\circ}\text{C}$, UV-poly at $T = 37\text{ }^{\circ}\text{C}$, and redox-poly at $T = 37\text{ }^{\circ}\text{C}$. These temperatures are close enough to the volume phase transition temperatures of the corresponding gels. The solid lines in the Figure denote theoretical fitting curves. As shown in the Figure, remarkable differences in $I(q)$ values were observed depending on the pH* for each type of gels. This

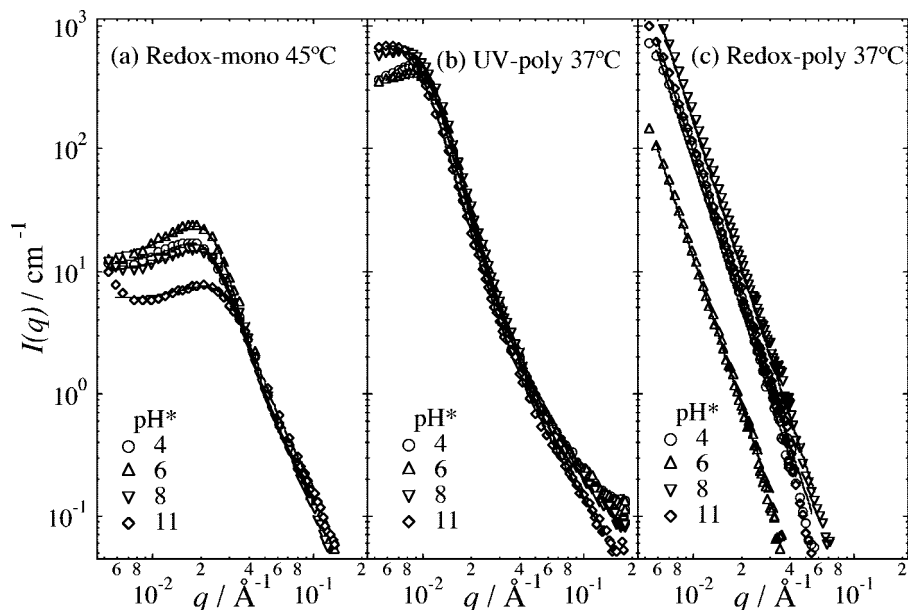


Figure 4. pH* dependence of SANS profiles at $T = 45\text{ }^{\circ}\text{C}$ for (a) redox-mono and at $T = 37\text{ }^{\circ}\text{C}$ for (b) UV-poly and (c) redox-poly. The solid lines denote the results of curve fitting.

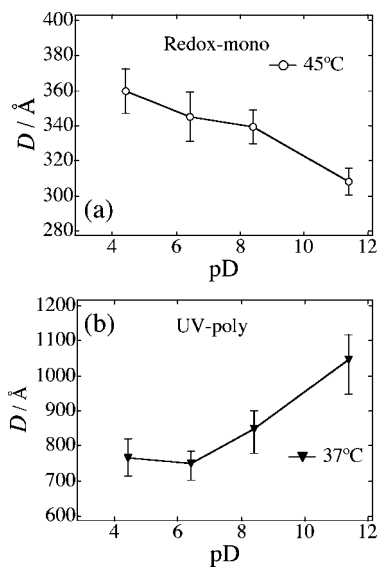


Figure 5. pD dependence of the periods of the repeat distance of microphase-separated structure, D , for (a) redox-mono and (b) UV-poly.

directly indicates that the difference in the distribution of charged groups significantly affects the microscopic network structures. In the case of redox-mono and UV-poly, scattering peaks appeared in $I(q)$ values in the low q region, indicating the existence of microphase separation. We note that the temperature at which microphase separation occurs in redox-mono is higher than that for UV-poly.²¹ This clearly means that a uniform distribution of AAc groups in redox-mono affects the microphase-separated structure of the polymer network more strongly than does a blocky distribution of AAc in UV-poly. In the case of redox-mono, these peaks remarkably shifted toward a higher q region by increasing the pH* at not only $T = 45$ but also $T = 49\text{ }^{\circ}\text{C}$ (not shown here), reflecting the microscopic structural changes in the microphase-separated state. In addition, because the peak position of UV-poly is very low ($q \approx 0.01\text{ }\text{\AA}^{-1}$), a microphase separation with a longer periodicity must be present. To reproduce these peaks in redox-mono and UV-poly, we employed RP theory. Here, the average degree of

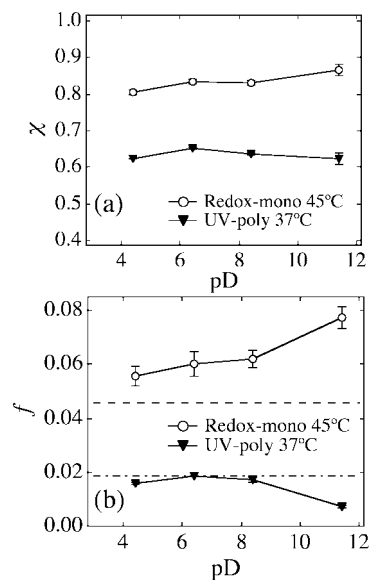


Figure 6. pD dependence of (a) the χ parameter and (b) the degree of charged AAc groups, f , for redox-mono and UV-poly.

polymerization between cross-links (N), the degree of ionized charged groups at sample preparation (f_0), and the polymer volume fraction (ϕ), were fixed at $N = 71$, $f_0 = 0.0457$, and $\phi (= \phi_0) = 0.1$ for redox-mono and $N = 417$, $f_0 = 0.0184$, and $\phi (= \phi_0) = 0.1$ for UV-poly.²¹ In the case of redox-poly at $37\text{ }^{\circ}\text{C}$, a power law behavior with a slope of -4 (i.e., Porod law) was observed, showing that redox-poly was macroscopically phase-separated into polymer-rich and -poor domains with the sharp boundary without exhibiting any characteristic features originating from charged groups.

pD Dependence of Structural Parameters. Figure 5 shows the pD ($= \text{pH}^* + 0.41$) dependence of the characteristic length at microphase-separated states, $D (= 2\pi/q_{\text{max}})$ for redox-mono and UV-poly. As shown in Figure 4, UV-poly underwent microphase separation with a longer period length of D than that of redox-mono. For redox-mono, D monotonically decreased with the increase in pD. This indicates that the $\text{p}K_a$ of AAc in redox-mono is larger at $45\text{ }^{\circ}\text{C}$ than at $25\text{ }^{\circ}\text{C}$, resulting

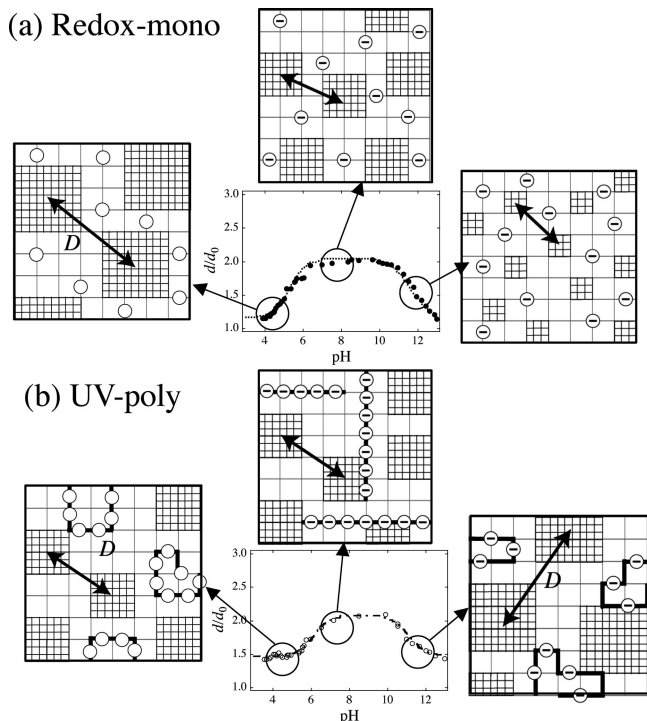


Figure 7. Schematic models explaining the pH dependence of microscopic network structure in conjunction with the pH dependence of the macroscopic swelling degrees at $T = 25\text{ }^{\circ}\text{C}$ for (a) redox-mono and (b) UV-poly.

in a noticeable change in *D*. The pD dependence of *D* for UV-poly is explained as follows. UV-poly underwent phase separation even when poly-AAc was not charged (pD = 4). This is probably the phase separation between hydrophilic poly-AAc domains and hydrophobic poly-NIPAm matrix. At pD of 8 and 11, screening effects are already dominant enough to enhance the concentration fluctuations in UV-poly, giving a larger *D* value. The difference in the pD dependence of the structural parameters between redox-mono and UV-poly is discussed in the following section.

Figure 6 shows the pD dependence of χ and *f* obtained from the curve fitting. The broken and chain lines in Figure 6b indicate the fraction of AAc groups in the polymer networks at sample preparation for redox-mono and UV-poly, respectively. It is well known that the χ parameter for the NIPAm aqueous system increases with temperature. Regarding Figure 6a, the following facts can be drawn. First, the fact that $\chi > 0.5$ clearly means that both redox-mono and UV-poly are in a poor solvent regime. Second, there is little or no pD dependence of χ , as expected. As for the pD dependence of *f* (Figure 6b), the following features were observed. For redox-mono, *f* increased with pD. With increasing pD up to 8, the effective degree of ionization of AAc increases because of dissociation. Moreover, *f* dramatically increased at pD of 11. This means that, unlike UV-poly, the apparent ionization degree of AAc groups increased without the occurrence of the screening effect by Na⁺. This is conjectured to the hydrolysis of amide groups under the strong basic condition, as reported elsewhere.^{55–58} We note that NIPAm polymer can be more strongly affected by hydrolysis in the case of redox-mono than by that in the case of UV-poly. This is because amide groups in NIPAm of redox-mono are more easily attacked by OH[−] because of the uniform distribution of AAc groups in the monomer unit, as also represented by the low inhomogeneities in Figure 3a. In the case of UV-poly, NIPAm networks rather form globule structures, as represented by the scattering profiles in Figure 3b. Because of the formation of the globule structures, the possibility

of attack by OH[−] can be small. As for the pD dependence of *f* for UV-poly, *f* remains constant up to a pD of 8. As discussed above, however, UV-poly is susceptible to the screening effect of Na⁺ because of the localization of AAc groups. As a result, the apparent degree of ionized AAc groups decreases at pD 11.

Figure 7 shows the schematic models that explain the pH dependence of the microscopic network structure at elevated temperatures (i.e., 37 or 45 °C) in conjunction with the pH dependence of the macroscopic swelling degree at $T = 25\text{ }^{\circ}\text{C}$ for redox-mono and UV-poly. Note that swelling curve measurements as a function of pH at the elevated temperatures were not possible because of the irreversible contraction of gels at low pHs. In Figure 7a,b, the NIPAm globules shrunk by hydrophobic interactions are designated by the dense lattice-shaped networks, and the characteristic distance of microphase separation, *D*, is shown by outward arrows. AAc monomers are designated by open circles with/without minus signs, whereas poly-AAc chains are designated as an array of open circles with bold solid lines. In the case of a, redox-mono is slightly charged at pH 4 and hence microphase separation is observed. By increasing pD, the ionization degree of AAc increases and *D* decreases to pH 10. However, at pH 11, more NIPAm globules are generated with the smaller size because of the hydrolysis of amide groups in NIPAm, resulting in the decrease in *D*.^{55,58}

In the case of UV-poly (Figure 7b), the microphase-separated structure is observed at pD of 4 and 6 where poly-AAc is noncharged or slightly charged. This results from phase separation between poly-AAc-rich domains and the poly-NIPAm matrix. By increasing the pH, the ionization effect of poly-AAc chains is effectively screened by added Na⁺, and *D* increases.

Concluding Remarks

The pH dependence of the structure and dynamics of three types of NIPAm/AAc gels with different spatial configurations of charged AAc groups was investigated by macroscopic swelling measurement and SANS. The pH dependences of the swelling degree for these gels were observed with the occurrence of the dependence of AAc distribution. The swelling degree profiles were well fit with the theoretical calculations by considering the additional cross-linking effects due to the chain entanglement. In addition, the ionization tendency of each gel was estimated by the comparison of obtained p*K*_a values. The SANS results indicate that there were no remarkable pD dependences at 25 °C, irrespective of the gel architecture. However, remarkable microscopic structural changes appeared in the microphase-separated state, showing clear pD dependences of the scattering peaks for redox-mono and UV-poly, respectively. For redox-mono, the characteristic length of microphase separation, *D*, decreased with pD, indicating ionization of charged groups and hydrolysis of amide groups in NIPAm under strong basic condition. For UV-poly, *D* increased with pD as a result of the screening effect by Na⁺. Curve fitting with the RP theory disclosed different pD dependences of *f* depending on the distribution of AAc groups. That is, *f* for redox-mono increased with pD, whereas that for UV-poly remained unchanged up to pD 8 and then decreased. In contrast, only redox-poly showed no pD dependence about microscopic inhomogeneities because of the physical entrapment of poly-AAc chains.

Acknowledgment. This work was supported by the Ministry of Education, Science, Sports and Culture, Japan (Grant-in-Aid for Scientific Research (A), 2006–2008, no. 18205025, and for Scientific Research on Priority Areas, 2006–2010, no. 18068004). The SANS experiment was performed with the approval of Institute for Solid State Physics of the University of Tokyo (proposal no. 6557) at Japan Atomic Energy Agency, Tokai, Japan.

References and Notes

- (1) Hirotsu, S.; Hirokawa, Y.; Tanaka, T. *J. Chem. Phys.* **1987**, *87*, 1392–1395.
- (2) Shibayama, M.; Tanaka, T. *Adv. Polym. Sci.* **1993**, *109*, 1–62.
- (3) Schosseler, F.; Skouri, R.; Munch, J. P.; Candau, S. J. *J. Phys. II* **1994**, *4*, 1221–1239.
- (4) Shibayama, M.; Ikkai, F.; Inamoto, S.; Nomura, S.; Han, C. C. *J. Chem. Phys.* **1996**, *105*, 4358–4366.
- (5) Borue, V.; Erukhimovich, I. *Macromolecules* **1988**, *21*, 3240–3249.
- (6) Rabin, Y.; Panyukov, S. *Macromolecules* **1997**, *30*, 301–312.
- (7) Sasaki, S.; Maeda, H. *J. Chem. Phys.* **1997**, *107*, 1028.
- (8) Flory, P. J. *Principles of Polymer Chemistry*; Cornell University Press: Ithaca, NY, 1953.
- (9) Lifshitz, I. M.; Grosberg, A. Y.; Khokhlov, A. R. *Rev. Mod. Phys.* **1978**, *50*, 683.
- (10) Richa, J.; Tanaka, T. *Macromolecules* **1984**, *17*, 2916.
- (11) Moe, S. T.; G, S.-B.; Elgsaeter, A.; Smidsrod, O. *Macromolecules* **1993**, *26*, 3589.
- (12) Panyukov, S.; Rabin, Y. *Phys. Rep.* **1996**, *269*, 1–132.
- (13) Shibayama, M. *Macromol. Chem. Phys.* **1998**, *199*, 1–30.
- (14) Mallam, S.; Horkay, F.; Hecht, A. M.; Geissler, E. *Macromolecules* **1989**, *22*, 3356.
- (15) Ikkai, F.; Shibayama, M. *Phys. Rev. E* **1997**, *56*, R51–R54.
- (16) Shibayama, M.; Norisuye, T.; Nomura, S. *Macromolecules* **1996**, *29*, 8746–8750.
- (17) Shibayama, M.; Takata, S.; Norisuye, T. *Phys. A* **1998**, *249*, 245–252.
- (18) Cohen, Y.; Ramon, O.; Kopelman, I. J.; Mizrahi, S. *J. Polym. Sci., Polym. Phys. Ed.* **1992**, *30*, 1055–1067.
- (19) Shibayama, M.; Tanaka, T.; Han, C. C. *J. Chem. Phys.* **1992**, *97*, 6842–6854.
- (20) Ikkai, F.; Shibayama, M.; Han, C. C. *Macromolecules* **1998**, *31*, 3275.
- (21) Ikkai, F.; Suzuki, T.; Karino, T.; Shibayama, M. *Macromolecules* **2007**, *40*, 1140–1146.
- (22) Suzuki, T.; Ikkai, F.; Shibayama, M. *Macromolecules* **2007**, *40*, 2509–2514.
- (23) Hirokawa, Y.; Tanaka, T. *J. Chem. Phys.* **1984**, *81*, 6379–6380.
- (24) Treloar, L. R. G. *The Physics of Rubber Elasticity*, 3rd ed.; Clarendon Press: Oxford, UK, 1975.
- (25) Hasa, J.; Ilavsky, M.; Dusek, K. *J. Polym. Sci., Polym. Phys. Ed.* **1975**, *13*, 253–262.
- (26) Shibayama, M.; Shirota, Y.; Hirose, H.; Nomura, S. *Macromolecules* **1997**, *30*, 7307.
- (27) Tanford, C. *Physical Chemistry of Macromolecules*; Wiley: New York, 1961.
- (28) Rice, S. A.; Nagasawa, M. *Polyelectrolyte Solutions: A Theoretical Introduction*; Academic Press: New York, 1961.
- (29) Katchasky, A.; Spitnik, P. *J. Polym. Sci.* **1947**, *2*, 432–446.
- (30) Seno, M.; Lin, M. L.; Iwamoto, K. *Colloid Polym. Sci.* **1991**, *269*, 873.
- (31) Panyukov, S.; Rabin, Y. *Macromolecules* **1996**, *29*, 7960.
- (32) Panyukov, S.; Rabin, Y. *Macromolecules* **1996**, *29*, 8530–8537.
- (33) Kubota, K.; Fujishige, S.; Ando, I. *Polym. J.* **1990**, *22*, 15–20.
- (34) Ikkai, F.; Adachi, E. *Macromol. Rapid Commun.* **2004**, *25*, 1514–1517.
- (35) Ikkai, F.; Shibayama, M. *Polymer* **2007**, *48*, 2387–2394.
- (36) Ikkai, F.; Adachi, E. *Macromol. Chem. Phys.* **2007**, *208*, 271–276.
- (37) Okabe, S.; Nagao, M.; Karino, T.; Watanabe, S.; Adachi, T.; Shimizu, H.; Shibayama, M. *J. Appl. Crystallogr.* **2005**, *38*, 1035–1037.
- (38) Shibayama, M.; Norisuye, T.; Ikkai, F. *J. Phys. Soc. Jpn., Suppl. A* **2001**, *70*, 306.
- (39) Covington, A. K.; Paabo, M.; Robinson, R. A.; Bates, R. G. *Anal. Chem.* **1968**, *40*, 700–706.
- (40) *CRC Handbook of Chemistry and Physics*; Lide, D. R., Ed.; CRC Press: Boca Raton, FL, 2000; Vol. 81.
- (41) Manning, G. S. *J. Chem. Phys.* **1969**, *51*, 934–938.
- (42) Manning, G. S. *J. Chem. Phys.* **1969**, *51*, 924–933.
- (43) Gundogan, N.; Melekaslan, D.; Okay, O. *Macromolecules* **2002**, *35*, 5616–5622.
- (44) Xue, W.; Champ, S.; Huglin, M. B. *Polymer* **2001**, *42*, 3665–3669.
- (45) Xue, W.; Huglin, M. B.; Jones, T. G. *J. Eur. Polym. J.* **2005**, *41*, 239–248.
- (46) Gundogan, N.; Okay, O.; Oppermann, W. *Macromol. Chem. Phys.* **2004**, *205*, 814–832.
- (47) Orakdogan, N.; Okay, O. *Eur. Polym. J.* **2006**, *42*, 955–960.
- (48) Chen, Z.; Cohen, C.; Escobedo, F. A. *Macromolecules* **2002**, *35*, 3296.
- (49) Tokuyama, H.; Ishihara, N.; Sakohara, S. *Eur. Polym. J.* **2007**, *43*, 4975–4982.
- (50) Nasimova, I. R.; Karino, T.; Okabe, S.; Nagao, M.; Shibayama, M. *J. Chem. Phys.* **2004**, *121*, 9708–9715.
- (51) Shibayama, M.; Isono, K.; Okabe, S.; Karino, T.; Nagao, M. *Macromolecules* **2004**, *37*, 2909–2918.
- (52) Horkay, F.; Hecht, A.-M.; Grillo, I.; Bassar, P. J.; Geissler, E. *J. Chem. Phys.* **2002**, *117*, 9103–9106.
- (53) Hecht, A. M.; Duplessix, R.; Geissler, E. *Macromolecules* **1985**, *18*, 2167.
- (54) Shibayama, M.; Tanaka, T.; Han, C. C. *J. Chem. Phys.* **1992**, *97*, 6829–6841.
- (55) Takata, S.; Norisuye, T.; Shibayama, M. *Macromolecules* **1999**, *32*, 3989–3993.
- (56) Miller, G.; Fenyo, J. C.; Selegny, E. *J. Appl. Polym. Sci.* **1980**, *25*, 627.
- (57) Park, T. G.; Hoffman, A. S. *J. Appl. Polym. Sci.* **1992**, *46*, 659.
- (58) Wang, X.; Li, Y.; Chang, W. *Anal. Chim. Acta* **1999**, *400*, 135.

MA801042Q